Viser Technology Pte. Ltd.
Mechanical Engineering Science
DOI: 10.33142/mes.v3i2.6725

Research Article Open Access

Influence of Different Equations of State on Simulation Results of Supercritical CO_2 Centrifugal Compressor

Yueming YANG[1], Bingkun MA[1], Yongqing XIAO[1], Jianhui QI[1,2*]

1 Shandong Engineering Laboratory for High-efficiency Energy Conservation and Energy Storage Technology & Equipment, School of Energy and Power Engineering, Shandong University, Jinan, China
2 Beijing Key Laboratory of Multiphase Flow and Heat Transfer for Low Grade Energy Utilization, North China Electric Power University, Beijing, China

***Corresponding Author:** *QI Jian-hui, No. 17923 Jingshi Road, Jinan, China; j.qi@sdu.edu.cn*

Abstract:
Supercritical CO_2 (SCO_2) Brayton cycle has received more and more attention in the field of power generation due to its high cycle efficiency and compact structure. SCO_2 compressor is the core component of the cycle, and the improvement of its performance is the key to improving the efficiency of the entire cycle. However, the operation of the SCO_2 compressor near the critical point has brought many design and operation problems. Based on the Reynolds Averaged Navier-Stokes (RANS) model, the performance and flow field of SCO_2 centrifugal compressors based on different CO_2 working fluid models are numerically investigated in this paper. The stability and convergence of the compressor steady-state simulation are also discussed. The results show that the fluid based on the Span-Wanger (SW) equation can obtain a more ideal compressor performance curve and capture a more accurate flow field structure, while the CO_2 ideal gas is not suitable for the calculation of SCO_2 centrifugal compressors. But its flow field can be used as the initial flow field for numerical calculation of centrifugal compressor based on CO_2 real gas.
Keywords: *Supercritical CO_2; Centrifugal compressor; Near the critical point; Compressor performance; Real gas equation of state*

Table 1 Prime table

Nomenclature		Subscripts	
r	Radius	0	Stagnation temperature or pressure
b	Width	1	Main blade inlet
η	Isentropic efficiency	2	Impeller exit
ε	Pressure ratio	3	Splitter blade inlet
p	Static pressure	t	Tip
T	Static temperature	s	Shroud
m	Mass flow rate	h	Hub
N	Impeller rotation speed	c	Critical state
V	Specific volume	u	General gas symbol
R	Gas constant		
w	Eccentricity factor.		
M_r	Molecular weight		
f	Helmholtz free energy		

1 Introduction

As a rapidly developing country, China has become the world's largest energy consumption country. In a long time to come, coal will still be the primary energy consumption. However, the massive consumption of fossil leads to problems such as climate warming and pollution, which have had a significant impact on the sustainable development of our country. In 2020, China officially committed to peak carbon dioxide emissions before 2030 and achieve carbon neutrality before 2060. The reduction of carbon emissions, the use of clean energy, and the improvement of energy efficiency have been included in the national strategy. The power system bridges human society and energy resources, and every gain on efficiency will make a great breakthrough in energy-saving and emission reduction. Using an advanced power cycle is one method to enhance the power system efficiency.

Supercritical CO_2 (SCO_2) Brayton cycle is a

Copyright © 2021 by author(s) and Viser Technology Pte. Ltd. This is an Open Access article distributed under the terms of the Creative Commons Attribution-NonCommercial 4.0 International License (http://creativecommons.org/licenses/by-nc/4.0/), permitting all non-commercial use, distribution, and reproduction in any medium, provided the original work is properly cited.
Received on October 13, 2021; Accepted on December 9, 2021

promising power cycle with great potential. SCO_2 is used as a working fluid in the cycle and no phase transition occurs during heating and cooling stages. Moreover, SCO_2 has the characteristics of large specific heat and low dynamic viscosity under operating conditions, which can realize thermal energy conversion more efficiently. The cycle not only has great application value in fossil energy power generation[1] but also has broad prospects in nuclear power[2], geothermal energy[3], solar power generation[4], and waste heat recovery[5]. However, in addition to high efficiency, another advantage of the SCO_2 Brayton cycle is that it has a more compact structure size. Due to its miniaturized system components and compact configuration, it has advantages for restricted space and weight applications, such as marine ships and interspace power systems [6]. However, the performance of some system components restricts the development and application of SCO_2 power systems, such as turbomachinery. Turbomachinery, including turbines and compressors, are the most important components in the SCO_2 power cycle. Sharp changes in fluid properties introduce greater uncertainties into experimental measurements and affect the accuracy of numerical simulations. This uncertainty becomes more prominent when the operating conditions approach the critical point. The most affected by the critical point physical properties of the system component is the compressor [7]. Hence, the SCO_2 compressor needs more attention.

As illustrated in previous studies, for lower power SCO_2 Brayton cycles, centrifugal compressors perform better than axial compressors in terms of stability and efficiency [8-9]. The study by Angelino and Invernizzi showed that the efficiency of both the SCO_2 compressor and the cycle increases when the compressor inlet conditions get near the CO_2 critical point [10]. Thus, keeping the operating point near the CO_2 critical point is essential for SCO_2 compressors, which helps reduce the compression work. However, Lee et al. proved that the dramatic changes in the thermodynamic properties of CO_2 near the critical point will lead to very high uncertainty in the prediction of compressor performance through experiments [11]. Kim et al. indicated that when the operating point approaches the critical points, the errors between numerical simulations and experiments will be increased [12]. Bao Wen-rui studied the internal flow structure of the SCO_2 centrifugal compressor at different inlet temperatures, and recommended an optimized inlet temperature for the off-design conditions [13]. Currently, the three-dimensional (3D) computational fluid dynamics (CFD) simulation is the most popular method for analyzing turbomachinery performance. Exploring the physical properties of the fluid in the SCO_2 centrifugal compressor and expanding the stability of the compressor are the focus of related research. Therefore, it is important to ensure the accuracy of the CO_2 thermophysical property model, and guarantee the convergence and stability of the solution process. This is necessary to optimize the design of SCO_2 centrifugal compressors.

This paper carries out a numerical simulation of a centrifugal compressor in a 350 kW SCO_2 power cycle. In the first part of the paper, brief descriptions of the studied compressor and computational domain are provided. Then, the numerical methodology and method verification are discussed. And the effect of RGP table resolution on the compressor performance is investigated. Finally, explore the effects of different CO_2 thermophysical properties models on its performance and flow field, and discuss the convergence issues in the numeical solution process.

2 Studied Case

2.1 Research model

Table 2 Main design parameters for SCO_2 compressor impeller

Model parameters	Value
Exit blade height (b_2)/mm	a
Inlet shroud radius (r_{s1})/mm	6.55a
Inlet hub radius (r_{h1})/mm	4a
Outlet radius (r_{t2})/mm	19.25a
Tip clearance(constant)/mm	0.15a
Inlet blade angle at tip/ °	58
Number main and splitter blades/-	8

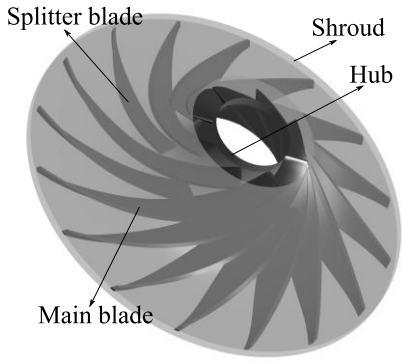

Figure 1 The 3D schematic of the SCO_2 compressor impeller

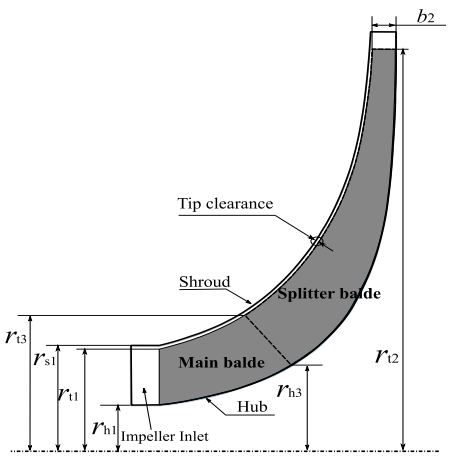

Figure 2 Meridional view of compressor's impeller

In this study, a single-stage centrifugal compressor is studied. As it is temporarily unable to disclose all design parameters, this article parameterizes the main size parameters, as shown in Table 2. As shown in

Figure1, the computational domain of the compressor impeller is generated by the modeling software SolidWorks. The meridional view of the impeller passage is shown in Figure2. The centrifugal compressor impeller consists of 8 main blades and 8 splitter blades. The designed mass flow rate (m) of the compressor is 6.4 kg/s, and the designed rotational speed (N) is 40,000 r/min.

2.2 Grid scheme

As shown in Figure3, a high-quality structured mesh of the impeller single passage was generated with ANSYS TurboGrid. For the reason that the blade tip clearance has an obvious influence on the flow field of the compressor, the mesh on the gap region was refined. Similar, it is necessary to ensure sufficient numbers of cells near the wall, so that the value of y+ for the first layer of near-wall-grid was between 1 and 5.

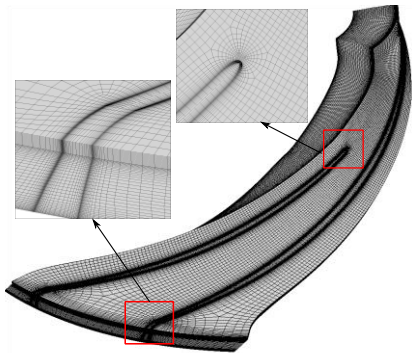

Figure 3 Single passage computational grid of the impeller

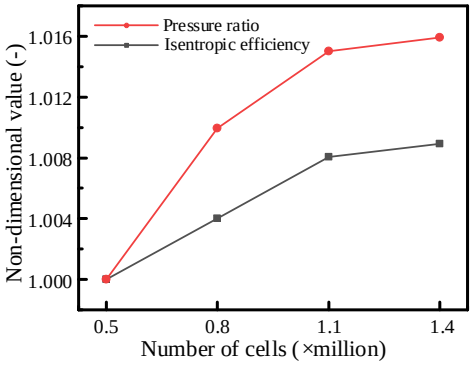

Figure 4 Schematic diagram of grid independence verification results

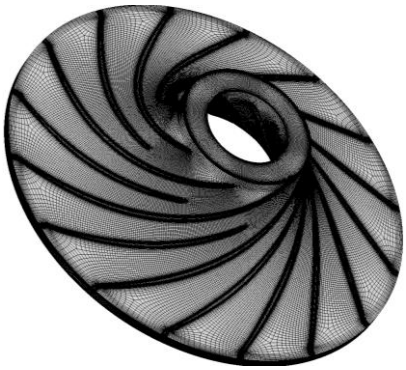

Figure 5 Computational grid of the impeller

The grid independence study was carried out with four different grid sizes. The number of cells for a single passage varies from 0.5 to 1.4 million with an increment of 0.3 million. For centrifugal compressors, we usually use pressure ratio (ε) and isentropic efficiency (η) to show their performances. These two parameters were used as monitored variables for the grid independence verification. Figure 4 shows the mesh dependency test for the studied centrifugal compressor. If the number of grids continues to increase after 1.1 million, the dimensionless values of the ε and η were both in the order of 10^{-3}, but the calculation speed dropped sharply. Therefore, a single-passage grid scheme with 1.1 million cells was adopted. And then import the grid into ICEM CFD to generate a full-passage grid scheme. The average $y+$ is 1.6 for the impeller single passage, which is in the reasonable range. Figure 5 shows the final computational grid scheme of the SCO_2 centrifugal compressor.

3 Methodology

3.1 Numerical method and boundary conditions

In this study, the commercial software ANSYS CFX[14] was used to simulate the 3D steady-state flow of the compressor. The solver adopts the finite volume method (FVM) based on finite elements, which not only guarantees the conservation characteristics of the finite volume method but also absorbs the numerical accuracy of the finite element method.

The internal flow of the compressor is very complicated, including many separated flows. Therefore, the turbulence model adopted the k-ω Shear Stress Transport (k-ω SST) model, which predicts the flow (such as separated flow) against the pressure gradient more accurately. The uniform m and total temperature ($T01$) were imposed at the compressor inlet boundary condition. The static pressure ($p2$) was imposed at the compressor outlet. The reference pressure was set to zero, and no slip-wall was employed on any solid wall. The high-resolution method was used at advection scheme and turbulence numerics. The convergence limit residual value of each physical quantity was set to 10^{-5}.

3.2 Validation through SNL's experiments

To validate the ability of ANSYS-CFX on solving the fluid field of the SCO_2 compressor, a SCO_2 compressor of Sandia National Laboratory (SNL) was simulated. The simulation results are used to compare with the experimental data. Table 3 shows the main parameters of the SNL compressor [15]. The characteristics of the small and high-speed SNL's compressor are similar to those of the SCO_2 centrifugal compressor in this study. Based on the ANSYS Workbench platform, BladeGen was used to generate a main compressor impeller model. TurboGrid was used to produce a high-quality structured grid. And CFX was used to perform steady-state calculations. The geometric model of the impeller reproduced during the verification process is provided in Figure 6. In terms of simulation settings, the

in-house Python code was used to invoke the CO_2 real gas properties in NIST REFPROP, and the k-ω SST model was also used to close the control equation. Table 4 lists other simulation condition settings.

Table 5 illustrates the difference between the simulation results and the experiments. The efficiency obtained from simulation is 70.1 %, which is 2.3 % higher than the experimental results, 67.8%. The pressure ratio is 1.20, which is identical to the experimental data. This fully proves the rationality of the simulation process in this research.

Table 3 SNL's compressor impeller parameters

Impeller Parameters	Value
Inlet shroud radius (r_{s1})/mm	9.372
Inlet hub radius (r_{h1})/mm	2.537
Outlet radius (r_{t2})/mm	18.681
Exit blade height (b_2)/mm	1.712
Inlet blade angle at tip/ °	50
Blade tip angle (minus is backswept)/ °	-50
Blade thickness/mm	0.762
Number main and split blades/-	6

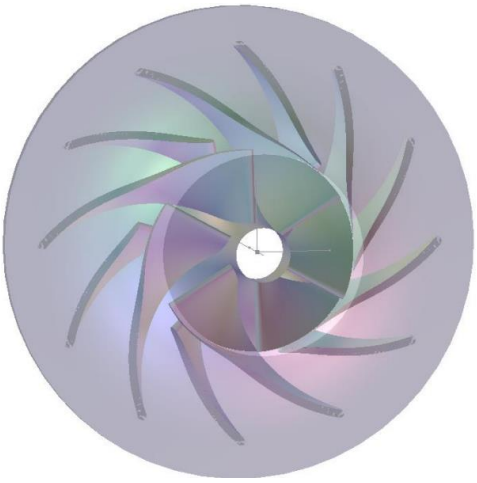

Figure 6 The 3D geometric model of SNL's compressor impeller

Table 4 SNL's compressor simulation settings

Location	Settings
Impeller inlet	p_{01} = 7.687 MPa T_{01} = 305.3 K
Computing domain outlet	m = 3.53 kg/s
Rotation speed	N = 50,000 r/min
Wall	Adiabatic、No Slip Wall
Working fluid	CO_2 Real Gas (Based on NIST REFPROP)

Table 5 Comparison of simulation results and experimental results

	Efficiency (η)/%	Pressure ratio (ε)/-
CFD	70.1	1.20
Laboratory data	67.8	1.20

4 Results and Analysis

To explore the influence of different CO_2 thermophysical properties models and real gas effects on the flow performance and flow field of SCO_2 compressors, this paper constructed three SCO_2 physical properties working fluid models, including CO_2 ideal gas model, CO_2 real gas model based on cubic Aungier-Redlich-Kwong equation of state (RK EoS), and CO_2 real gas property model based on Span-Wanger equation of state (SW EoS). The compressor used these three working fluids for steady-state numerical calculation.

4.1 CO_2 ideal gas property model

SCO_2 is assumed to be an ideal gas, and the thermodynamic process in the compressor satisfies the following equation:

$$pV = R_g T \tag{1}$$

$$pV^{\kappa} = C \tag{2}$$

κ is the isentropic index which is the ratio of the specific heat capacity at constant pressure and the specific heat capacity at a constant volume. For an ideal CO_2 gas, κ = 1.29, C is a constant.

The performance of the CO_2 ideal gas model for centrifugal compressors was studied below. In order to facilitate the comparison with the data based on the real gas model, the simulation used the same T01 and p01. Figure 7 shows that the compressor surges at the mass flow rate of about 1.8 kg/s under the designed rotational speed. This is consistent with the simulation results because the relevant calculation error occurs at a 1.8 kg/s flow rate. The flow choking phenomenon will occur when m reaches about 5.2 kg/s, and related errors will also appear in the ANSYS CFX solver. Compressor simulated with ideal gas models cannot reach the design m of 6.4 kg/s. In the actual operation of the compressor, the temperature and pressure of the working fluid in the impeller will increase from the inlet to the outlet. The density of ideal gas changes linearly with temperature and pressure, and it can be considered that the density changes little. However, for CO_2 real gas, the density near the critical point varies dramatically with temperature and pressure and will reach a larger value. Therefore, m of the compressor with ideal gas as working fluid cannot reach the design m of real gas working fluid. In addition, with the increase of m, the decrease of ε almost decreases at the same rate, which conforms to the performance curve shape of the general centrifugal compressor. However, for the performance curve where the η varies with m, the highest efficiency point appears near the surge flow rate, which is not in line with the actual situation.

In summary, when CO_2 ideal gas is used as the working fluid of the compressor, the real gas effect cannot be exerted. The performance of the compressor will be reduced significantly compared with the real refrigerant compressor. For the entire Brayton cycle, it will become an important factor in reducing cycle efficiency.

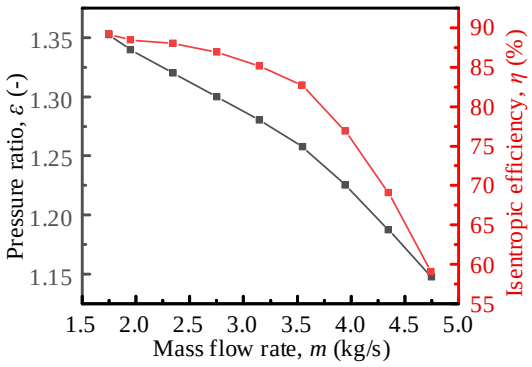

Figure 7 Performance curve of the centrifugal compressor based on CO_2 ideal gas

4.2 CO_2 real gas property models

4.2.1 Real gas calculated by RK EoS

Compared with other real gas EoS, the cubic EoS has the advantages of fewer variables, greater flexibility, and higher accuracy. These equations are widely used in engineering applications. One of them is RK EoS. The fluid based on CO_2 RK EoS is used in this study comes from the ANSYS CFX database. Its thermophysical properties are calculated using the Aungier-Redlich-Kwong cubic EoS [16]. The formula is shown in the appendix.

4.2.2 Real gas calculated by SW EoS

Span and Wanger proposed a multi-parameter state equation of CO_2 physical properties based on Helmholtz free energy [17]. Because of the wide range of applications, this equation can more accurately capture the changes in the thermal properties of CO_2 in the supercritical region and near the critical point. At the same time, due to closer to the experimental measurement data, it is recommended by the National Institute of Standard and Technology. The equation consists of the ideal part and the remaining part, and it is shown in the appendix.

4.2.3 RGP table based on SW EoS

An RGP file combining the NIST REFPROP database was encoded and employed for numerical analysis to deal with the dramatic variation of CO_2 thermophysical properties. Import the generated physical property parameter table (RGP table) into the ANSYS CFX solver to define a new working fluid. The bilinear interpolation method was used to calculate the thermophysical properties. It can be seen that the higher the resolution of the RGP tables, the more accurate the simulation. Especially at the adjacent region of the critical point, the thermodynamic properties of CO_2 change drastically with the variation of temperature and pressure. However, if the resolution of the physical property table is too high, it will have a large effect on the stability and convergence of the numerical calculation of the SCO_2 compressor [18]. ANSYS CFX solver has limited memory capacity to read the RGP table. So, if the resolution is too high, the table will not be read. Considering the above facts, an optimum resolution of the table will have to be found.

Similar to the grid-independent study, the pressure ratio and isentropic efficiency of the centrifugal compressor were used as the monitor in the dependency study of RGP tables. In this study, the RGP table ranges 250-450 K and 3-30 MPa for temperature and pressure, respectively. Six RGP tables have various resolutions from 50×50 up to 800×800 points. Same boundary conditions are assigned to the simulation cases with different table resolutions. The boundary condition settings are listed in Table 6. In order to express the changes intuitively, a nondimensional value was obtained by dividing the simulated performance data by the simulated data of the highest resolution table calculation results. Figure 8 shows the independent study results of the RGP table. As the resolution increases, the total pressure ratio rises gradually, and the isentropic efficiency shows a trend of oscillation convergence. When the resolution exceeds 400×400, the performance of the SCO_2 compressor tends to be steady. But, when the resolution is lower than 400×400, the simulation becomes unstable and the error becomes significant. Considering the stability, convergence, and accuracy of the simulation, RGP tables with a resolution of 400×400 are used.

Table 6 Boundary conditions applied to the independent study of RGP table resolution

Location	Boundary Conditions
Impeller inlet	T_{01} = 306.15 K m = 6.4 m/s
Computing domain outlet	p_2= 12 MPa
Rotation speed	N = 12,000 r/min
Working fluid	CO_2 Real Gas (Based on NIST REFPROP)

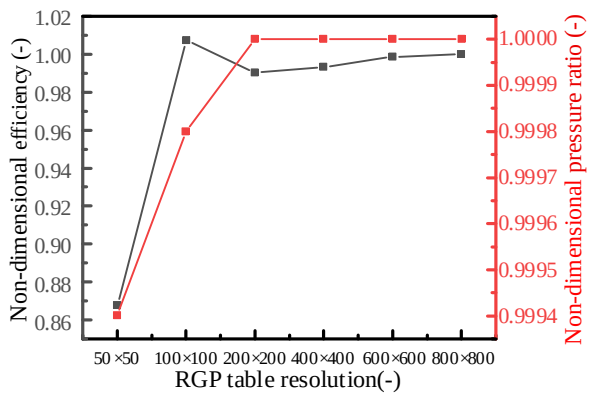

Figure 8 Accuracy of the RGP tables

A study on the convergence and stability of the RGP table with different resolutions at various compressor rotation speeds is also carried out, as shown in Figure9. If the number of convergence steps is equal to zero, it indicates the simulation is divergent at this speed. At the same speed, with the resolution of the RGP table increasing, the convergence steps of the simulation increase, which is more difficult to converge. This is

because, when the rotational speed increases, the temperature and pressure near the leading edge will decrease. Thus, it is easier that the fluid properties drop into the metastable region below the critical point. This makes it difficult to calculate physical properties with drastic changes in physical properties

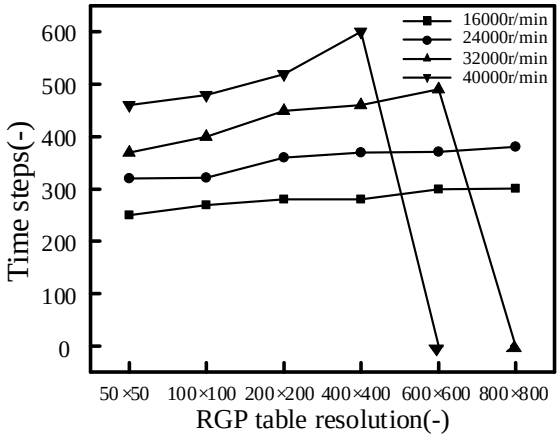

Figure 9 Stability test of RGP tables with different resolutions at different rotational speeds

To increase the convergence rate of the simulation, this study tries to initialize the flow field with simulation results of the ideal gas. Figure 10 compares the average residual convergence curves of the momentum equation with and without initialized flow field. It can be seen that after initializing the flow field, the convergence speed of numerical simulation is greatly improved, and the convergence residual is smaller. So, it is necessary to initialize the flow field for the following simulation with real gas.

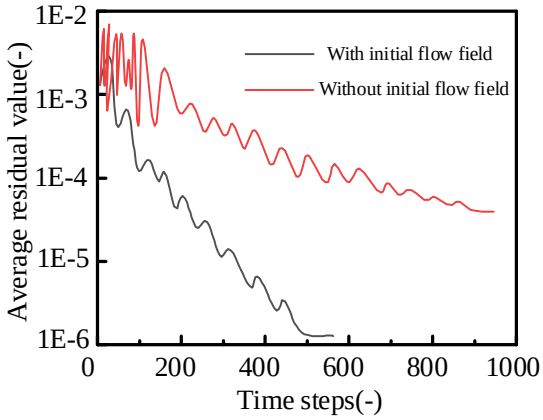

Figure 10 Convergence history of momentum equation with or without initialization

4.3 Comparison of two real gas EoSs

To explore the influence of two sets of real gas EoSs on the steady-state simulation of SCO_2 centrifugal compressor, the ε of compressors calculated by two real gas EoSs under four different speeds are compared in this paper, as shown in Figure11. With the increase of rotational speed, the ε is also increasing. However, the ε calculated with RK EoS is lower than that calculated by SW EoS. Besides, with the increase of rotational speed, the gap between the ε of the two increases gradually. The reason for this phenomenon is that the calculation accuracy of the cubic EoS in the near-critical and supercritical regions is inferior to the Helmholtz free energy EoS [19]. After many iterations, the error accumulates, which leads to the inability for simulations near the critical point and supercritical state. As the speed increases, the pressure and temperature near the leading edge of the blade drop to a position closer to the critical point due to local acceleration. However, near the critical point, the RK EoS will produce greater calculation errors. Compared with the ideal gas, the performance of the centrifugal compressor calculated by the steady-state numerical simulation of the CO_2 real gas based on the RK EoS is still greatly improved.

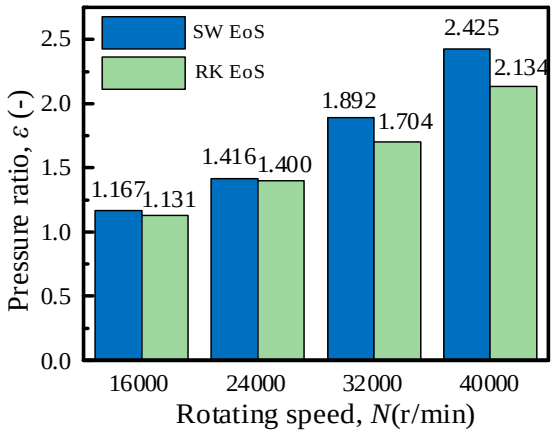

Figure 11 Comparison of the pressure ratio of two CO_2 real gas property models under steady-state simulation calculations at different speeds

The flow fields of the simulation with two CO_2 real gas EoSs are compared and analyzed in Figure12. The x-axis indicates the normalized streamwise position, and 0 is the entrance, 1 is the exit. From the entrance to the exit, the temperature and pressure will show an overall increase. There are local fluctuations in thermodynamic properties near the leading edge due to the flow separations, which leads to a certain level of losses. In Figure12 (a), the static pressure and total pressure of fluid calculated by RK EoS are higher than fluid calculated by SW EoS at the inlet, but along the streamwise direction, the difference between the two working fluid parameters is gradually reduced. At the exit, the total pressure of CO_2 real gas calculated by SW EoS has exceeded that calculated by RK EoS, and the static pressure level is very close. In Figure12 (b), the difference between the total temperature and static temperature of the CO_2 real gas calculated by SW EoS has exceeded that calculated by RK EoS. Observing the operating fluid parameter level, we can see that the working fluid calculated by the SW EoS shows better operating performance at a fixed speed.

Figure 13 illustrates the distributions of streamlines in the impeller internal passage of the centrifugal compressors. In the tip clearance of the main blade and the splitter blade, the phenomenon of flow across the tip clearance is normal. The flow velocity increases in the tip clearance and the flow across the tip clearance is

more obvious in the latter half of the blade. More swirls form in the passage when the fluid calculated by RK EoS crosses the tip clearance, which leads to easier flow separation and more losses. The position of the vortex is marked by a red line frame in Figure13. It can be seen that the low-speed area caused by the vortex in the flow field of RK EoS is significantly larger than that in the flow field of SW EoS. This also explains the reason why the parameter curve of RK EoS is lower than that of SW EoS in Figure12. In other words, this is an important reason that the performance of a centrifugal compressor with CO_2 real gas based on SW EoS is better than that with CO_2 real gas based on RK EoS.

Figure 14 shows the pressure distribution near the leading edge of the blade when the compressor operates on three different working fluids. Both the CO_2 ideal gas flow field and the CO_2 real gas flow field will show a pressure drop at the leading edge of the blade. The pressure drop of the ideal gas is relatively gentle and small, and the pressure is above the critical pressure. The pressure drop of the real gas flow field is drastic, especially for the flow field based on the SW EoS. The pressure in a considerable part of the area has dropped below the critical point (pressure lower than 7.38 MPa). The profile curvature at the leading edge of the main blade changes the most, so the fluid velocity gradient also increases. The fluid velocity increased dramatically, resulting in a distinct low-pressure and low-temperature region at the leading edge of the main blade. In other words, the phenomenon of flow acceleration at the leading edge of the compressor impeller will cause the working fluid to enter the two-phase region. A criterion for determining whether condensation of supercritical carbon dioxide has occurred deserves further discussion. It can also be observed that the pressure rise near the tip of the blade leading edge due to flow impact is also more intense in a real gas. The Mach number and entropy contours at 80% span are presented in Figure 15. As can be seen from the Mach number contour, the flow acceleration occurs at the leading edge of the blade suction side. Since entropy increase is an important sign of flow loss, it can be seen from the entropy contour that the existence of the two-phase region has produced a larger loss.

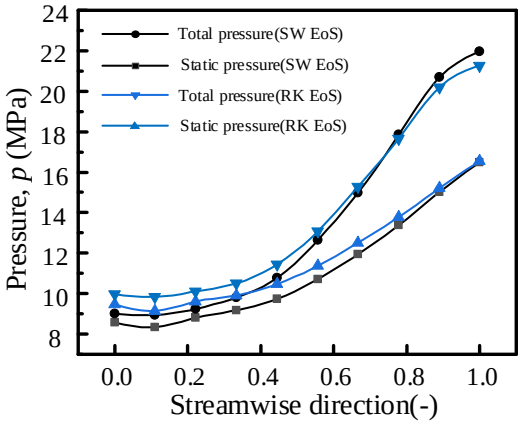

(a) Pressure change in streamwise direction

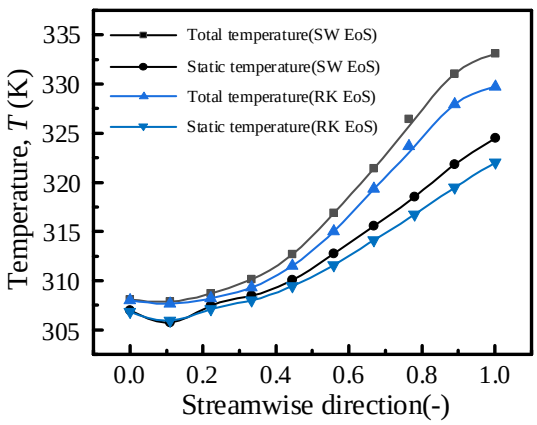

(b) Temperature change in streamwise direction

Figure 12 Schematic diagram of the temperature and pressure changes of the compressor in the streamwise direction calculated by two different EoSs

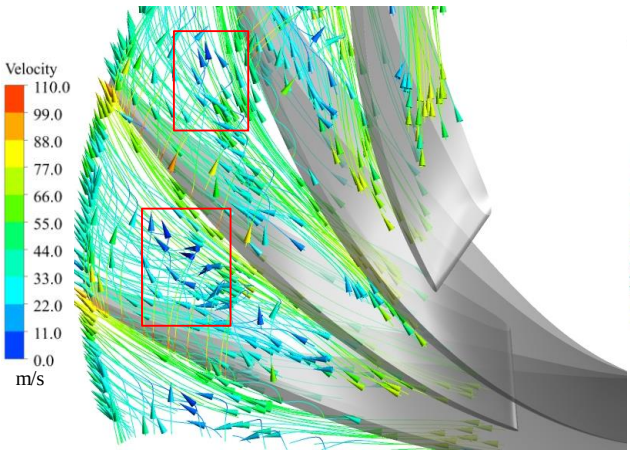

(a) Streamline distribution of impeller passages with RK EoS

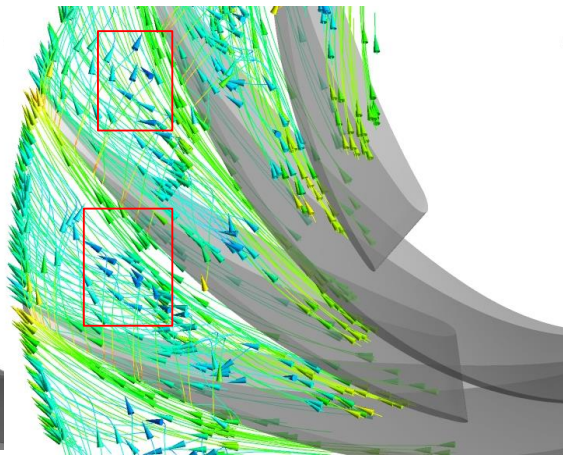

(b) Streamline distribution of impeller passages with SW EoS

Figure 13 The streamline distribution of compressor impeller passages based on two different CO_2 real gas EoSs

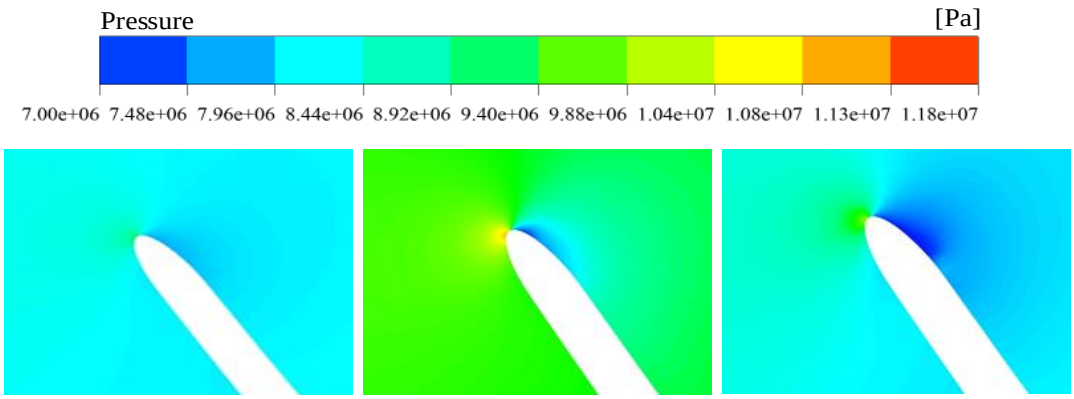

(a) Blade leading edge with CO_2 ideal gas (b) Blade leading edge with RK EoS (c) Blade leading edge with SW EoS

Figure 14 Schematic diagram of the pressure distribution on the leading edge of the blade at 80% span

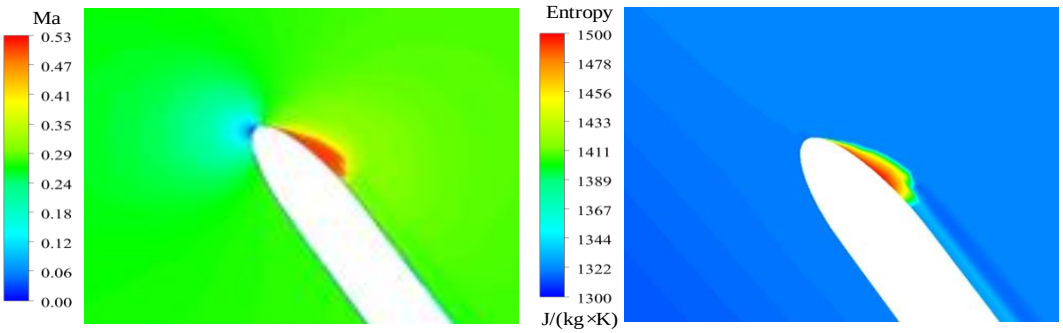

(a) Mach number (b) Entropy

Figure 15 Mach number and entropy contours at 80% span

5 Conclusion

This study explores the influence of three different gas EoSs on the steady-state simulation characteristics of SCO_2 centrifugal compressor, and the main conclusions are as follows:

(1) Analyzing the ideal gas simulation results, it can be seen that the performance is poor and can only work under a small mass flow rate. When applying ideal gas EoS, the simulated compressor working range is 1.8-4.8kg/s; the highest isentropic efficiency can only reach 88%; the highest pressure ratio is about 1.35. When the simulation result of the ideal gas is used as the initial condition of the real gas simulation, it will have a good effect.

(2) In this study, the external RGP tables were combined with the computational fluid dynamics solver. Through the independent study of the RGP table resolution, a table with 400 × 400 is selected to carry out the following simulations. The drastic change of CO_2 thermodynamic properties near the critical point has a certain impact on the stability and convergence characteristics of the numerical simulations. By the stability analysis, it can be found that as the RGP table resolution and simulated rotational speed increase, the possibility of simulation divergence increases.

(3) By analyzing and comparing the effects of two real gas EoS on the simulated performance and flow field of SCO^2 centrifugal compressors, it is found that the RK EoS has certain errors in the calculation of physical properties near the critical point. In the front half of the flow passage of the impeller, especially the position of the leading edge of the blade, some phenomena in the flow field based on RK EoS cannot be captured. Besides, the simulation based on RK EoS predicts a higher flow loss in the latter half of the blade.

Conflict of Interest: The authors declare that there is no conflict of interest regarding the publication of this paper.

Acknowledgments: Funding data: National Natural Science Foundation of China (Grant No: 52106049); Natural Science Foundation of Shandong Province (ZR2020QE191); Natural Science Foundation of Jiangsu Province (BK20210113); The Young Scholars Program of Shandong University (31380089964175).

Appendix A.

CO_2RK EoS:

$$p=\frac{RT}{V-e+c}-\frac{\alpha(T)}{V(V+e)} \tag{1}$$

$$\alpha(T)=d\left(\frac{T_c}{T}\right)^n \tag{2}$$

$$c=\frac{RT_c}{p_c+d/(V_c^2+V_c\cdot e)}+e-V_c \tag{3}$$

$$n=0.4986+1.1735w+0.4754w^2 \tag{4}$$

$$d=0.42747R^2T_c^2/p_c \tag{5}$$

$$e=0.08664RT_c/p_c \tag{6}$$

$$R = \frac{R_u}{M_r} \tag{7}$$

In formula (4), d and e are constants, used to correct the intermolecular gravitation and correct the volume respectively. A fourth-order polynomial was used for the calculation to ensure simulation accuracy.

CO_2SW EoS:

$$\frac{f(\rho,T)}{R_g T} = \phi(\delta,\tau) = \phi^0(\delta,\tau) + \phi^r(\delta,\tau) \tag{8}$$

In formula (11), ϕ is the Helmholtz free energy nondimensionalized by the gas constant and temperature. δ and τ are the reciprocals of the relative density and relative temperature respectively. The relative value here is relative to the critical point. ϕ^0 and ϕ^r represent the ideal part and the remaining part of the physical properties of CO_2, respectively.

$$\phi^0(\delta,\tau) = \ln(\delta) + a_1^0 + a_2^0\tau + a_3^0\ln(\tau) + \sum_{i=4}^{8} a_i^0 \ln(1-e^{-\tau\theta_i^0}) \tag{9}$$

Where a_i^0 and θ_i^0 are the parameters of the ideal part.

$$\phi^r = \sum_{i=1}^{7} n_i\delta^{di}\tau^{ti} + \sum_{i=8}^{34} n_i\delta^{di}\tau^{ti}e^{-\tau c_i} + \sum_{i=35}^{39} n_i\delta^{di}\tau^{ti}e^{-\alpha_i(\delta-\epsilon_i)^2-\beta_i(\tau-\gamma_i)^2} + \sum_{i=40}^{42} n_i\Delta^{bi}\delta e^{-C_i(\delta-1)^2-D_i(\tau-1)^2} \tag{10}$$

In formula (13), α_i, β_i, γ_i, ϵ_i, t_i, c_i, b_i, C_i, D_i, and n_i are all the parameters of i≤39 in the remaining part. The improvement of the calculation accuracy of physical properties near the critical point by this equation is mainly derived from the last term in formula (13).

$$\Delta = \left\{(1-\tau) + A_i[(\delta-1)^2]^{\frac{1}{2\beta_i}}\right\}^2 + B_i[(\delta-1)^2]^{a_i} \tag{11}$$

In formula (14), ai, βi, Ai, and Bi are all parameters of 39≤i≤42 in the remaining part, and they are all constants. In the SW EoS, other thermophysical parameters need to be calculated by Helmholtz free energy and its partial derivatives relative to temperature and density, such as pressure, enthalpy, entropy, and so on.

References

[1] Jia-Qi Guo, Ming-Jia Li, Jin-Liang Xu,et al. Energy, exergy and economic (3E) evaluation and conceptual design of the 1000 MW coal-fired power plants integrated with S-CO_2 Brayton cycles[J]. Energy Conversion and Management,2020,211.

[2] Vaclav Dostal, Pavel Hejzlar, Michael J Driscoll. High-Performance Supercritical Carbon Dioxide Cycle for Next-Generation Nuclear Reactors[J]. Nuclear Technology,2006,154(3).

[3] Eduardo Ruiz-Casanova, Carlos Rubio-Maya, J Jesús Pacheco-Ibarra,et al. Thermodynamic analysis and optimization of supercritical carbon dioxide Brayton cycles for use with low-grade geothermal heat sources[J]. Energy Conversion and Management,2020,216.

[4] Qi Jian-hui, Reddell Thomas, Qin Kan,et al. Supercritical CO_2 Radial Turbine Design Performance as a Function of Turbine Size Parameters[J]. Journal of Turbomachinery,2017,139.

[5] Xu-rong Wang, Yi-ping Dai. Exergoeconomic analysis of utilizing the transcritical CO 2 cycle and the ORC for a recompression supercritical CO_2 cycle waste heat recovery: A comparative study[J]. Applied Energy,2016,170.

[6] Vaclav Dostal, Pavel Hejzlar, Michael J. Driscoll. The Supercritical Carbon Dioxide Power Cycle: Comparison to Other Advanced Power Cycles[J]. Nuclear Technology,2006,154.

[7] Nikola D. Baltadjiev, Claudio Lettieri, Zoltan S. Spakovszky. An Investigation of Real Gas Effects in Supercritical CO_2 Centrifugal Compressors[J]. Journal of Turbomachinery,2015,137(9).

[8] Zhi-yuan Liu, Weiwei Luo, Qing-jun Zhao,et al.Preliminary Design and Model Assessment of a Supercritical CO_2 Compressor[J]. Applied Sciences,2018,8(4).

[9] Darryn Fleming, Thomas Holschuh, Tom Conboy,et al. Scaling Considerations for a Multi-Megawatt Class Supercritical CO_2 Brayton Cycle and Path Forward for Commercialization[C]. Copenhagen, DENMARK: ASME Turbo Expo 2012.

[10] Angelino G, Invernizzi C. Real Gas Brayton Cycles for Organic Working Fluids, Proceedings of the Institution of Mechanical Engineers, Part A: Journal of Power and Energy. 2001,215(1); pp. 27-28.

[11] Jekyoung Lee, Seungjoon Baik, Seong Kuk Cho,et al. Issues in performance measurement of CO_2 compressor near the critical point[J]. Applied Thermal Engineering,2016,94.

[12] Seong Gu Kim, Jekyoung Lee, Yoonhan Ahn,et al. CFD investigation of a centrifugal compressor derived from pump technology for supercritical carbon dioxide as a working fluid[J]. The Journal of Supercritical Fluids,2014,86.

[13] Bao Wen-rui, Yang Ce, Wang Wen-li,et al. Effect of inlet temperature on flow behavior and performance characteristics of supercritical carbon dioxide compressor[J]. Nuclear Engineering and Design,2021,380.

[14] ANSYS Academic Research, ANSYS CFX User Guide, Release 17.1, ANSYS, Inc, 2016

[15] Wright, Steven A, Lipinski,et al. Closed Brayton Cycle Power Conversion Systems for Nuclear Reactors: Modeling, Operations, and Validation. The United States,2006.

[16] Aungier R H. A Fast, Accurate Real Gas Equation of State for Fluid Dynamic Analysis Applications[J]. Journal of Fluids Engineering,1995, 117:277-281.

[17] Roland Span, Wolfgang Wagner. A New Equation of State for Carbon Dioxide Covering the Fluid Region from the Triple-Point Temperature to 1100 K at Pressures up to 800 MPa[J]. Journal of Physical and Chemical Reference Data,2009,25(6).

[18] Ameli Alireza, Afzalifar Ali, Turunen-Saaresti,et al Effects of Real Gas Model Accuracy and Operating Conditions on Supercritical CO_2 Compressor Performance and Flow Field[J]. Journal of Engineering for Gas Turbines and Power-Transactions of the ASME,2018,140(6).

[19] Michela Mazzoccoli, Barbara Bosio, Elisabrtta Arato. Analysis and Comparison of Equations-of-State with p-ρ-T Experimental Data for CO_2 and CO_2-Mixture Pipeline Transport[J]. Energy Procedia,2012,23: 274-283.